J Mater Sci (2007) 42:1765–1771
DOI 10.1007/s10853-006-0895-9

Plastic flow stability of metallic nanolaminate composites

A. Misra · R. G. Hoagland

Received: 13 June 2006 / Accepted: 28 August 2006 / Published online: 16 December 2006

Abstract Metallic nanolaminate composites synthesized via physical vapor deposition possess ultra-high strengths, often within a factor of two to three of the theoretical strength limit, when the bilayer periods are on the order of a few nanometers. The origins of failure in vapor-deposited nanolaminate composites at large plastic strains have not been reported in any significant detail. In this article, we present an overview of the length-scale dependent plastic flow stability of metallic nanolaminates deformed to large plastic strains via room temperature rolling.

Introduction

Nanolaminate composites are made up of alternating nanometer-scale layers of two or more different materials, where the individual layer thickness can be varied from a few atomic layers to many nanometers. While the components of nanolaminates may be metals, metallic glass, intermetallics, or ceramics, the focus of this article will be on metal–metal systems. Nanolaminates have been the subject of significant recent research world wide due to the novel mechanical and physical properties that emerge as the individual layer thickness is reduced to nanometer-scale [1, 2]. For example, the yield strength of a Cu–Nb nanolaminate, at individual layer thickness of 2 nm, is on the order of 2.5 GPa, which is approximately a factor of two less than a lower bound estimate of the theoretical strength of a perfect crystal of either Cu or Nb ($\approx E/30$ where E is the Young's modulus [3]).

Much of the earlier work on nanolaminate materials was limited to evaluation of the mechanical properties via nano-indentation and/or tensile testing. For high strength materials, uniform elongation in tension is limited by the Considere criterion that predicts onset of necking when $d\sigma/d\varepsilon < \sigma$ where σ is the flow stress and $d\sigma/d\varepsilon$ is the work hardening rate [4]. Thus, it was not possible to explore features such as deformation texture, dislocation storage and recovery, work hardening, and plastic flow stability of the laminate composites due to the limited uniform elongation typically achieved in tensile testing. Recently we have studied deformation of vapor deposited nanolaminates to large plastic strains via room temperature rolling [5]. These experimental studies have been performed on a model Cu–Nb system. In a parallel study, the details of the interface structure and dislocation-interface interactions are being explored via atomistic modeling by Hoagland et al. [6].

In this article, we report on the plastic flow stability of Cu–Nb nanolaminates as a function of the individual layer thickness from around 4 nm to 4 μm. The observed stability or instability of plastic flow at large strains is interpreted in terms of the unit dislocation mechanisms that determine yield strengths.

A. Misra (✉) · R. G. Hoagland
Materials Science and Technology Division,
Los Alamos National Laboratory,
Los Alamos, NM 87545, USA
e-mail: amisra@lanl.gov

Experimental

Cu–Nb nanolaminates were synthesized by dc magnetron sputtering at room temperature on Si substrates.

After deposition, the multilayered thin foils were peeled off the substrates, cut into strips about 10 mm wide and 25 mm long, and sandwiched between two stainless steel sheets, each about 200 μm thick, for rolling. Other details of synthesis and rolling procedures are provided elsewhere [5, 7]. The rolling strains in this article are quoted as engineering strain corresponding to the layer thickness reduction, $(h_f - h_o)/h_o$ where h_f is the final layer thickness after rolling, and h_o is the initial layer thickness. The microstructures of the as-deposited and rolled foils were examined using transmission electron microscopy (TEM). Figure 1 shows a cross-section TEM image, with the corresponding selected area diffraction pattern of an as-deposited Cu–Nb nano-laminate along with the rolling geometry. The Cu and Nb layers exhibited the Kurdjumov–Sachs (KS) orientation relationship: {111}Cu//{110}Nb; ⟨110⟩Cu//⟨111⟩Nb, such that the interface plane is {111}Cu//{110}Nb. The grain structure is columnar and within each column, the in-plane directions ⟨111⟩Nb and ⟨110⟩Cu are parallel. However, there is no alignment of the in-plane K–S directions, ⟨111⟩Nb//⟨110⟩Cu, between adjacent column grain pairs. In other words, the column-to-column texture is random in-plane, as also deduced from the X-ray pole figure measurements [7].

Results

The observed length-scale dependence of the plastic flow stability of Cu–Nb nano-laminates as a function of the initial layer thickness ranging from 4 μm to 4 nm is described below. Three kinds of behavior were observed: (i) non-uniform reduction in layer thickness with dislocation cell structure formation for sub-micrometer to micrometer-scale initial layer thicknesses; (ii) uniform reduction in layer thickness with no dislocation cell structure formation for initial layer thickness below 100 nm, and (iii) layer thickness reduction interrupted by the formation of shear cracks for initial layer thickness below 10 nm.

Non-uniform reduction in layer thickness with cell structure formation

Cu–Nb micro-laminates with initial layer thicknesses of 4 μm (2 bilayers, total sample thickness = 16 μm), 2 μm (2 bilayers, total thickness = 8 μm) and 600 nm (6 bilayers, total thickness = 7.2 μm), respectively, were rolled to 50% reduction. All these samples exhibited similar behavior shown in Fig. 2. For a sample with initial layer thickness of 2 μm (Fig. 2a), the rolled microstructure shows non-uniform layer thickness reduction. Note that the as-deposited samples had flat interfaces. In Fig. 2a, the Cu/Nb interfaces are marked by dotted lines to highlight the heterogeneity in the deformation. In spite of the non-uniform thickness reduction, no layer pinch-off was observed. At significantly finer length scale of 600 nm (Fig. 2b), the heterogeneity in the layer thickness reduction is still apparent. Within the Cu and Nb layers, a very high density of dislocation tangles/networks was noted in the Nb layer, whereas in the Cu layer the dislocation structure was recovered to form a sub-grain cell structure comprising of dislocation boundaries with a significantly lower dislocation density within the cells. The behavior shown in Fig. 2 is typical of that of bulk metals. In other words, pure Cu or Nb rolled to 50% reduction develop dislocation cell structures quite similar to the micrometer-scale Cu and Nb layers within the multilayer. A related aspect

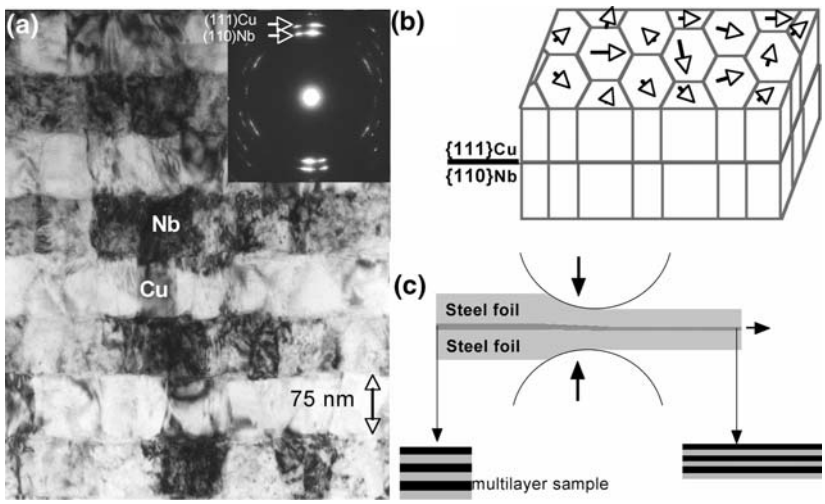

Fig. 1 (**a**) Cross-section TEM micrograph and corresponding selected area diffraction pattern of as-deposited Cu–Nb multilayer. The rolling direction is parallel to the layers. (**b**) Schematic of the texture between Cu and Nb. For a pair of columnar Cu and Nb grains across the interface, {111}Cu//{110}Nb// interface plane and ⟨110⟩Cu//⟨111⟩Nb. Arrows indicate the parallel ⟨110⟩Cu//⟨111⟩Nb directions that are random from one column to next, indicating random in-plane texture

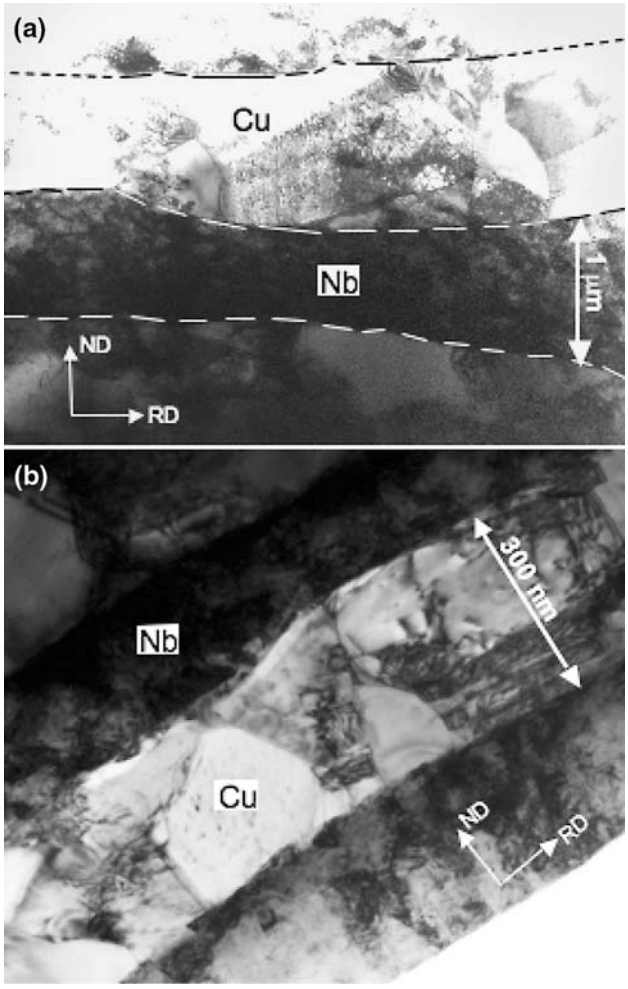

Fig. 2 Cross-section TEM micrographs of Cu–Nb micro-laminates rolled to around 50% layer reduction; (**a**) initial thickness of 2 μm, and (**b**) initial thickness of 600 nm. Note the non-uniform reduction in layer thickness and dislocation storage within the layers

was the development of bulk rolling textures in the Cu and Nb layers which destroyed the K–S orientation relationship in the as-deposited multilayers during rolling [7, 8].

Uniform reduction in layer thickness without cell structure formation

As the initial layer thickness was reduced to below ≈100 nm, significantly different behavior was observed. Cu–Nb nanolaminates with initial layer thickness of around 75 nm did not exhibit any sub-grains or tangles/networks of dislocations within the layers, even after ~60% reduction in rolling, and the Cu and Nb layers were reduced in thickness uniformly (Fig. 3). While a few dislocations could be discerned threading the layer thickness, such threading dislocation segments were observed in the as-deposited samples as well. Statistically, no significant change in the total dislocation density was observed even after 50% reduction. Quantitative analysis of X-ray diffraction line broadening also indicated insignificant increase in stored dislocation density after rolling [9]. Hence, despite the very different flow strengths and hardening rates of Cu and Nb single-phase materials, the alternating layers of Cu and Nb in nanoscale multilayers respond identically to the room temperature rolling with a uniform reduction in layer thickness. This is an indication that the length scale is small enough so that the plastic properties of the constituent phases in the bulk form do not play a role in determining the deformation behavior.

In addition to the significant difference in the dislocation storage in micro vs. nanolaminates, the deformation textures were also completely different. Figure 4a shows the {111} and {110} pole figures for Cu and Nb in the as-deposited Cu–Nb nanolaminates. The highest intensities in the centers of the {111}Cu and{110}Nb pole figures are consistent with the {111}Cu//{110}Nb// interface plane relationship shown in Fig. 1. During rolling of micro-laminates, the typical rolling textures for bulk fcc and bcc metals developed in the Cu and Nb layers respectively. An example is shown in Fig. 4b for a rolled micro-laminate with a 4 μm initial layer thickness. Note the significant splitting of the ⟨111⟩Cu interface plane normal along

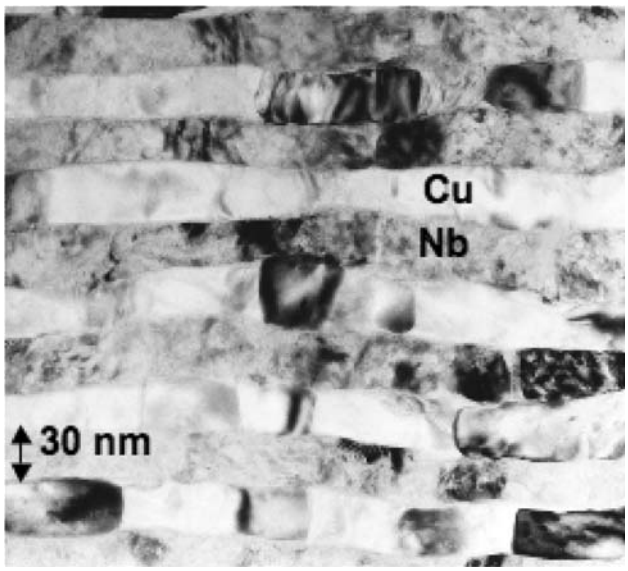

Fig. 3 Cross-section TEM micrograph of a Cu–Nb nano-laminate with initial layer thickness of 75 nm rolled to a final thickness of 30 nm. Note the uniform reduction in layer thickness and lack of any dislocation cell structures within the layers

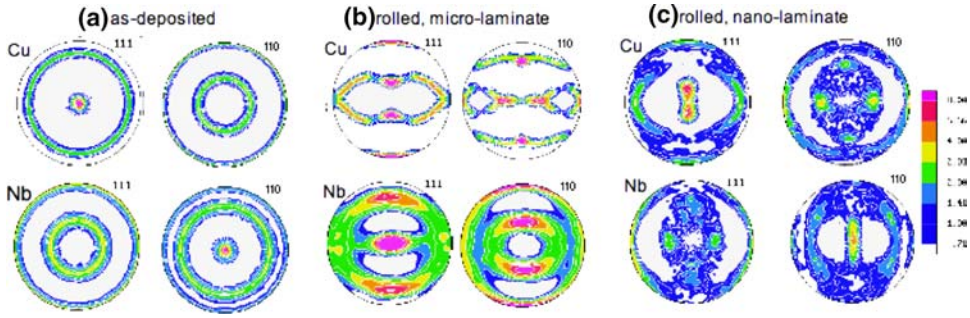

Fig. 4 Textures of (**a**) as-deposited, (**b**) rolled micro-laminates and (**c**) rolled nano-laminates of Cu–Nb [7]. Note the rotation away from the {111}Cu//{110}Nb// interface plane initial texture during rolling of micro-laminates but not in nano-laminates

the rolling direction, whereas for Nb the interface plane normal switches from ⟨110⟩ to near ⟨111⟩ during rolling. Thus, the initial Kurdjumov–Sachs orientation relations are lost during deformation. In contrast, in the rolled nanolaminates, the Kurdjumov–Sachs orientation relation was preserved during rolling. Figure 4c shows the rolling texture for a nano-laminate with a 75 nm initial layer thickness. Note that there has been very little rotation away from the interface normal. The pole figure measurements also showed (discussed elsewhere [7, 10]) that the in-plane ⟨111⟩ Nb//⟨110⟩ Cu directions remained parallel during rolling.

Deformability limited by the formation of shear cracks

Figure 5a is a plan view SEM micrograph showing through-thickness cracks in a rolled foil. This Cu–Nb nanolaminate had an initial layer thickness of 15 nm and was rolled to 50% reduction. For the case shown in Fig. 5a, the cracks were spaced about 50–100 μm (the total initial sample thickness was 7.5 μm) and were about 200 μm long, on average. With such a distribution of micro-cracks, the multilayered foil was perforated but the sample was still in one piece. Perhaps the most significant observation is that the fracture appears to be by shear cracks. The crack plane is not normal to the rolling direction, rather inclined and roughly along the planes of maximum shear stress, shown schematically in Fig. 5b.

For initial layer thickness of 4 nm, shear cracks were observed during the first rolling pass, set at a reduction of around 3%.

Enhanced deformability in bimodal multilayers

In contrast to the cracking in the 4 nm multilayers during the first rolling pass, bimodal multilayers with repeat periodicity of the four layer stack of 40 nm Cu/40 nm Nb/4 nm Cu/4 nm Nb exhibited no shear cracks after 20% reduction in rolling. TEM image of the rolled bimodal multilayer (Fig. 6) shows uniform reduction in layer thickness with no dislocation cell structure formation. The 4 nm thick Cu and Nb layers co-deformed with the 40 nm layers, i.e., no clear evidence of decohesion or shear cracking was observed. Energy dispersive spectroscopy line scan in a TEM with ≈1 nm probe size was also used to confirm the presence of chemically discrete ≈3 nm thick Cu and Nb layers in rolled multilayers.

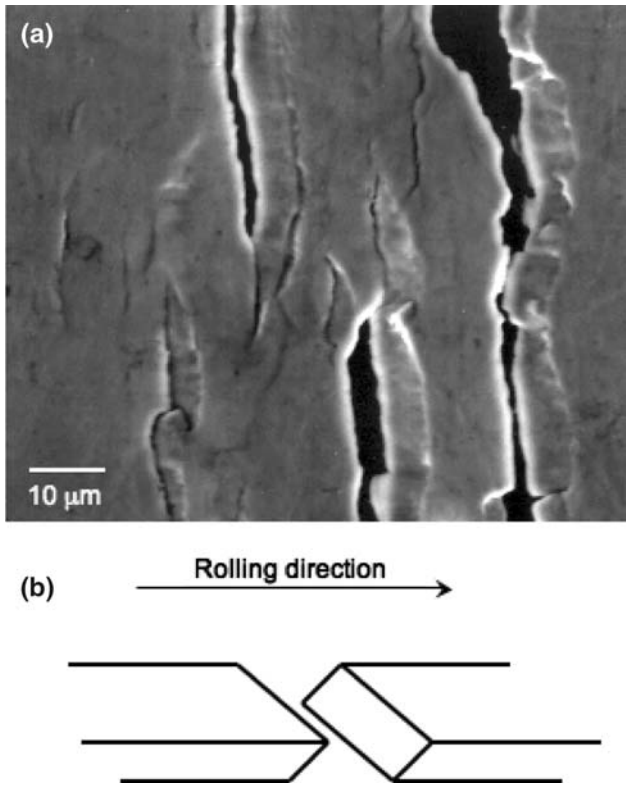

Fig. 5 (**a**) Plan view SEM image and (**b**) schematic showing through-thickness shear cracks in a Cu–Nb nano-laminate with initial thickness of 15 nm, rolled to around 50% reduction

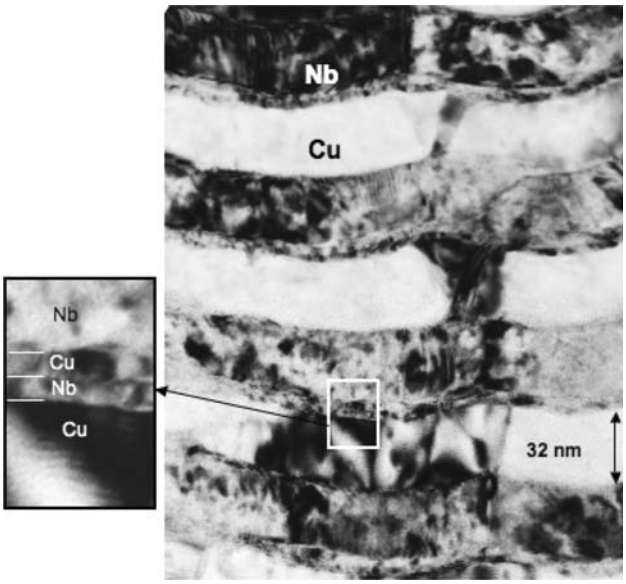

Fig. 6 Cross-section TEM micrograph of a bimodal 40 nm Cu–Nb/4 nm Cu–Nb multilayer rolled to approximately 20% reduction

Discussion

The plastic flow stability of the room temperature rolled Cu–Nb multilayers as a function of the initial layer thickness from 4 μm to 4 nm is discussed here in terms of the unit deformation mechanisms. First, we discuss the behavior at coarse length scales from sub-micrometer and higher. Here the key features are (i) non-uniform reduction in layer thickness but no layer pinch-off, (ii) the development of dislocation cell structure within the individual Cu and Nb layers, and (iii) development of rolling textures within the Cu and Nb layers such that the initial K–S orientation relationship is lost. The heterogeneity of deformation at this length scale can be interpreted in terms of the dislocation pile-up mechanism of deformation. The plastic shear is concentrated on the planes where dislocations glide in groups as pile-ups, and coupled with the stochastic nature of the activation of sources that lead to dislocation pile-ups results in non-uniformly spaced coarse slip bands. Thus, the layer thickness reduction is non-uniform. The plastic flow stability of bulk laminate composites fabricated by repeated rolling and pressing of alternate metal foils has been discussed in the literature [11–15]. Two kinds of behavior have been reported: (i) initial local heterogeneous deformation and multiple necking of one or more phases (but no layer pinch-off), and (ii) multiple fracture of the relatively harder phase such that the laminate composite evolves into a particulate morphology with increasing deformation.

The instability criterion as derived by Chen [11] is:

$$(\sigma_h - \sigma_s) > \frac{d}{d\varepsilon}(\sigma_h - \sigma_s)$$

where σ_h and σ_s are the respective flow stresses of the constituent phases, and $d/d\varepsilon$ is the difference in the work hardening rates of the two layers. This instability criterion is based on the flow stresses of the two phases in the monolithic, bulk forms and does not account for the length scale of the layers. For the case of bulk Cu and Nb, the difference between the respective flow stresses is presumably not large enough to result in multiple fracture of the Nb layer during rolling. Thus, for sub-micrometer and micrometer scale Cu–Nb multilayers, layered morphology is preserved during rolling although the reduction in layer thickness is non-uniform.

Next we discuss the homogeneous deformation of multilayers with initial layer thickness of a few tens of nanometers. At nanometer length scales, dislocation pile-ups may not form and the deformation behavior is controlled by the nucleation and motion of single dislocations. At layer thickness of a few tens of nanometers, the single dislocation mechanism is referred to as *confined layer slip* (Fig. 7) [3, 16, 17].

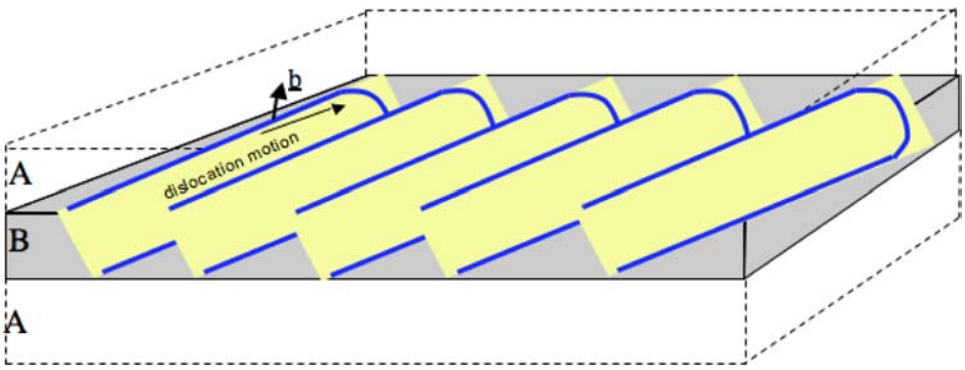

Fig. 7 Schematic of confined layer slip in an A/B multilayer. For simplicity, dislocations are shown in only one layer. Activation of confined layer slip on closely spaced parallel planes results in a uniform distribution of plastic strain along the layer length

There is co-deformation of Cu and Nb layers via single dislocation loops bounded by the interfaces and confined to glide in the respective Cu and Nb layers. The confinement of glide loops to individual layers is due to the fact that the interface barrier to slip transmission is higher than the confined layer slip stress. As shown in Fig. 7, each confined layer glide loop leads to the deposition of dislocation segments at the two bounding interfaces. The dislocations deposited at the interface would repel a possible like sign second dislocation on the same glide plane. Thus, the continued dislocation activity is more likely on other parallel slip planes. With increasing strain, these dislocations get distributed, more or less uniformly, along the interface. Since a glide dislocation also experiences repulsion from a like-sign dislocation on a closely spaced parallel plane, subsequent slip events are not localized at the site of the initial slip plane. This results in a uniformly spaced slip distribution and hence, uniform reduction in layer thickness. The process is analogous to the development of uniform spaced misfit dislocation arrays at interfaces that form in lattice-mismatched thin films on substrate via confined layer slip of glide dislocations in the strained film [18]. As shown in our earlier work [10], the preservation of interface crystallography after large plastic strains is due to activation of symmetric slip. In other words, multiple slip systems are activated with slip activities balanced such that the net out-of-plane rotation is nearly zero.

For confined layer slip, strength increases approximately as the inverse of the layer thickness. Thus, when the layer thickness is reduced to a few nanometers, the confined layer slip stress exceeds the interface barrier to slip transmission, resulting in a transition from confined layer slip to interface cutting by single dislocations. The disconnection created at the interface at the site of the slip transmission results in a shear offset (Fig. 8). For a layer thickness of around 4 nm, passage of several dislocations across the interface on the same slip plane is sufficient to shear the layer. The interface disconnection created by slip transmission tends to repel further slip activity on the same plane resulting in some level of work hardening, as shown by Hoagland and co-workers via atomistic modeling [19]. However, when the ratio of the shear offset to layer thickness exceeds some critical value, slip may become localized on that plane. This phenomenon is being explored in more detail via atomistic modeling and will be presented elsewhere. The strain localization in the 4 nm thick layers can be suppressed, to a significant extent, by the constraint from the relatively thicker 40 nm layers in bimodal multilayers. This is because in bimodal multilayers, the 40 nm layers yield first and develop a relatively uniform array of interface dislocations (of the kind shown in Fig. 7) by confined layer slip, thereby transferring load to the 4 nm layers. Note that the 40 nm layer thickness is thin enough to suppress the formation of long dislocation pile-ups. The slip transfer scenario for the bimodal multilayers is shown schematically in Fig. 9. Presumably the slip initiation sites in the 4 nm layers follow, as a 'template', the uniform array of interface dislocations developed in the 40 nm layers, leading to a uniform distribution of slip events in the thin layers, thereby suppressing shear localization. We are investigating the deformability of the bimodal multilayers where the volume fraction of the 4 nm layers (i.e., the number of 4 nm layers per 40 nm layer) is higher than the case shown in Fig. 6 and this will be discussed in a future article.

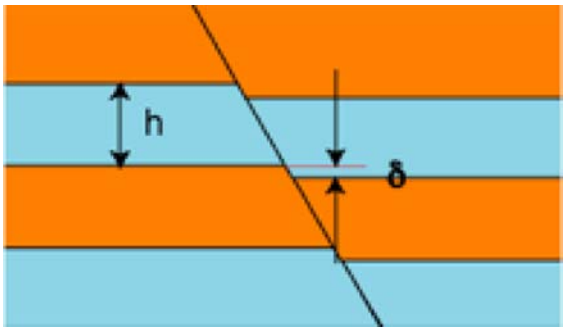

Fig. 8 Schematic of the shear location in nanolaminates caused by multiple slip transmission events across the interface on the same glide plane. When the ratio of the shear offset (δ) to the layer thickness (h) exceeds some critical value, slip may be localized on that plane

Summary

The dependence of plastic flow stability of metallic multilayers on the layer thickness is summarized in

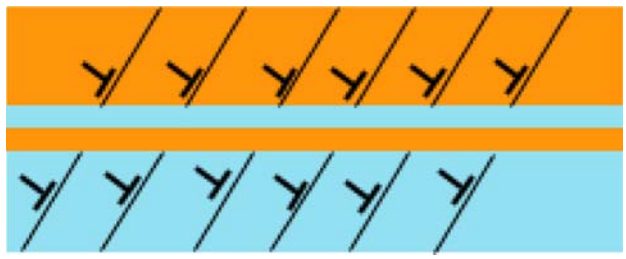

Fig. 9 Schematic of the slip transfer in bimodal multilayers where the thin layers are a few nanometers and the thick layers are a few tens of nanometers. Homogeneously distributed confined layer slip in thicker layers suppresses the number of interface crossing events through the thin layers on the same glide plane

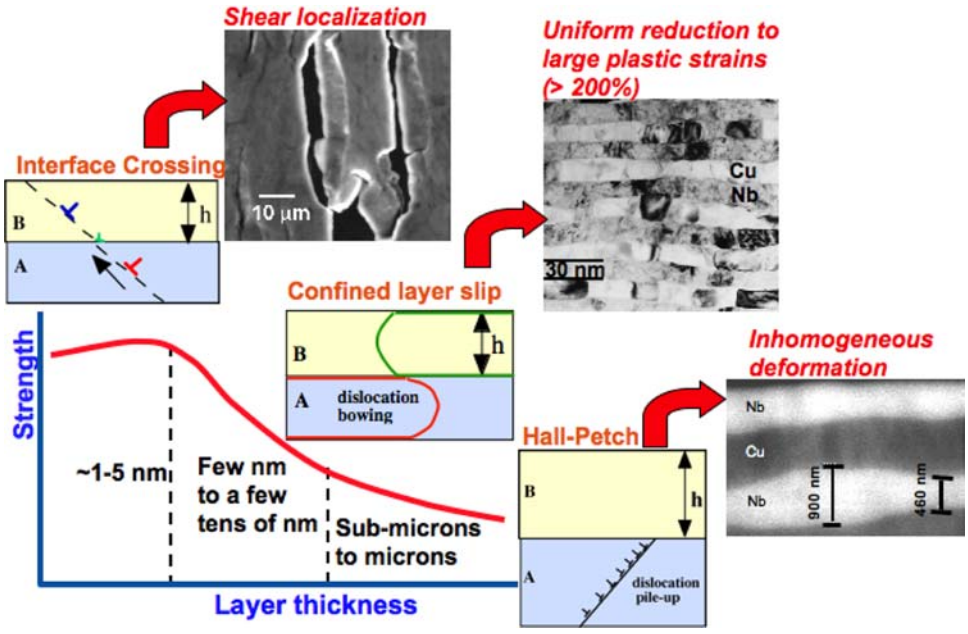

Fig. 10 Summary of the dependence of plastic flow stability of metallic multilayers on the layer thickness from micrometers to nanometers

Fig. 10. At sub-micrometer to micrometer length scales, dislocation pile-up based Hall–Petch mechanism is applicable in interpreting the layer thickness dependence of strength. Deformation via pile-ups of dislocations leads to heterogeneous distribution of slip and non-uniform reduction in layer thickness. At layer thickness of a few tens of nanometers, confined layer slip via single dislocations in both layers leads to uniform reduction in layer thickness with no dislocation cell structure formation and preservation of the initial crystallographic orientation relationship between Cu and Nb. At layer thickness of a few nanometers, the confined layer slip stress exceeds the interface barrier to slip transmission resulting in interface cutting and strain localization that limits the uniform deformability. The deformability at few nanometers can be enhanced by making bimodal multilayers that alternate few nanometer thick layers with a few tens of nanometers thick layers.

Acknowledgments This research is supported by the DOE, Office of Science, Office of Basic Energy Sciences. Authors acknowledge useful discussions with J.P. Hirth. J.D. Embury, H. Kung, and collaborations with J.F. Bingert, D.L. Hammon, C.N. Tome, X. Zhang, E. Vanderson, and K. Hattar.

References

1. Clemens BM, Kung H, Barnett SA (1999) MRS Bulletin 24:20
2. Scripta Materialia Viewpoint Set No. 34 titled Deformation and stability of nanoscale metallic multilayers, edited by A. Misra, J.D. Embury and H. Kung, vol. 50, No. 6, (2004)
3. Misra A, Hirth JP, Hoagland RG (2005) Acta Materialia 53(18):4817
4. Dieter GE (1986) Mechanical Metallurgy, 3rd edn. McGraw-Hill, Boston, p 286
5. Misra A, Kung H, Hammon D, Hoagland RG, Nastasi M (2003) Int J Damage Mech 12:365
6. Hoagland RG, Kurtz RJ, Henager CH Jr (2004) Scripta Materialia 50:775
7. Anderson PM, Bingert JF, Misra A, Hirth JP (2003) Acta Materialia 51:6059
8. Al-Fadhalah K, Tome CN, Beaudoin AJ, Robertson IM, Hirth JP, Misra A (2005) Philos Mag 85(13):1419
9. Nyilas K, Misra A, Ungar T (2006) Acta Materialia 54(3):751
10. Misra A, Hirth JP, Hoagland RG, Embury JD, Kung H (2004) Acta Materialia 52(8):2387
11. Chen IW, Winn EJ, Menon M (2001) Mat Sci Engg A317:226
12. Bordeaux F, Yavari R (1990) Z Metallkde 81:130
13. Hutchinson JW, Tvergaard V (1980) Int J Mech Sci 22:339
14. Steif PS (1987) J Appl Metal Work 4:317
15. Semiatin SL, Piehler HR (1979) Metall Trans 10A:97–107
16. Phillips MA, Clemens BM, Nix WD (2003) Acta Materialia 51:3157
17. Anderson PM, Foecke T, Hazzledine PM (1999) MRS Bulletin 24:27
18. Mitlin D, Misra A, Radmilovic V, Nastasi M, Hoagland RG, Embury JD, Hirth JP, Mitchell TE (2004) Philos Mag 84:719
19. Henager CH, Kurtz RJ, Hoagland RG (2004) Philos Mag 84:2277